Article

Visible-Light-Driven AO7 Photocatalytic Degradation and Toxicity Removal at Bi-Doped SrTiO$_3$

Maria João Nunes *[ID], Ana Lopes [ID], Maria José Pacheco [ID] and Lurdes Ciríaco

Fiber Materials and Environmental Technologies (FibEnTech-UBI), Universidade da Beira Interior, R. Marquês de D'Ávila e Bolama, 6200-001 Covilhã, Portugal; analopes@ubi.pt (A.L.); mjap@ubi.pt (M.J.P.); lciriaco@ubi.pt (L.C.)
* Correspondence: maria.nunes@ubi.pt

Abstract: In this study, Bi-doped SrTiO$_3$ perovskites (Sr$_{1-x}$Bi$_x$TiO$_3$, x = 0, 0.03, 0.05, 0.07 and 0.1) were synthesized using the solid-state method, characterized, and tested as photocatalysts in the degradation of the azo dye acid orange 7 (AO7) under visible light. The perovskites were successfully synthesized, and XRD data showed a predominant, well-crystallized phase, belonging to the cubic perovskite symmetry. For the doped samples, a minority phase, identified as bismuth titanate, was detected. All doped samples exhibited improved photocatalytic activity under visible light, on the degradation of AO7 (10 mg L^{-1}), when compared with the undoped SrTiO$_3$, with an increase in relative Abs$_{484\,nm}$ decay from 3.7% to $\geq$67.8% after 1 h, for a powder suspension of 0.2 g L^{-1}. The best photocatalytic activity was exhibited by the Sr$_{0.95}$Bi$_{0.05}$TiO$_3$ perovskite. Reusability studies showed no significant loss in photocatalytic activity under visible light. The final solutions showed no toxicity towards *D. magna*, proving the efficiency of Sr$_{0.95}$Bi$_{0.05}$TiO$_3$ as a visible-light-driven photocatalyst to degrade both the AO7 dye as well as its toxic by-products. A degradation mechanism is proposed.

Keywords: perovskite; Bi-doped SrTiO$_3$; visible light photocatalysis; AO7; toxicity

1. Introduction

Photocatalysis is a promising, clean process that can be applied in the degradation of persistent organic pollutants, such as organic dyes [1–6]. This process initiates with the irradiation of a suitable catalyst's surface with a type of radiation, i.e., UV, visible, or solar, with energy equal to or higher than the bang gap energy (E$_g$) value. If this prerequisite is met, the electrons of the valence band are excited to the conduction band, initiating a succession of reactions that culminate with the formation of highly reactive radical species, such as O$_2^{\bullet-}$ and OH$^\bullet$. These radical species will react with the organic molecules, breaking the bonds and generating intermediate metabolites and leading to, ideally, complete mineralization.

A photocatalyst can exhibit activity under visible light if its E$_g$ is narrow enough to be activated by visible radiation [7]. This facilitates the application of natural sunlight as the source of renewable energy, given that ~42% of the incident radiation falls under the visible wavelength, resulting in a more cost-effective and environmentally friendly process. Furthermore, the reuse of treated effluents can be implemented according to the European Union (EU) regulation 2020/741 "on minimum requirements for water reuse", for irrigation purposes and groundwater recharge [8].

Perovskite-type compounds, such as halide perovskites, have been studied as promising photocatalysts for some applications such as CO$_2$ reduction under UV–visible radiation [9] and PET–RAFT polymerization under visible and near-infrared radiation [10], due to their superior properties. Other types, such as perovskite oxides, have shown to be more suitable than their halide counterparts for application as catalysts in the photocatalytic degradation of aqueous solutions of several compounds, including organic dyes, due to their higher water stability [11–23]. These ceramic materials, with the general formula

ABO$_3$, are well known for their stable and flexible structure that allows the accommodation of several cationic combinations and consequent variety of properties. Strontium titanate (SrTiO$_3$) is a cubic perovskite oxide reported to exhibit photocatalytic activity under UV light [24,25]. This limitation is attributed to a wide energy gap of 3.0–3.2 eV [26–28] and hinders the application of low-cost solar light. One method to lower the energy gap value and increase the photoabsorption range of SrTiO$_3$ is element doping, due to its low cost and overall simplicity [29]. Hou et al. [30] and Liu et al. [31] reported that through the Cr-doping of SrTiO$_3$, E$_g$ of 2.32–2.12 eV and lower than 3.2 eV were obtained, respectively. Comparable lowering of E$_g$ of SrTiO$_3$ was also observed by doping it with Mn (2.76 eV) [32] and Bi (2.6 eV and 3.04 eV) [33,34].

Azo dyes are a widely used group of synthetic dyes, accounting for 60–70% of the global industry demand [35,36]. These dyes are characterized by the presence of the -N=N- chromophore in diverse complex aromatic structures and possess high chemical stability and breakdown resistance over time to sunlight radiation and microorganisms [37]. Due to these characteristics, conventional wastewater treatments are not always effective to achieve complete degradation of these compounds. Azo dyes' incomplete degradation could lead to the formation, and consequent release, of metabolites with higher toxicity than the parent dye molecule [36]. In the case of acid orange 7 dye, some of the degradation products are known to be more toxic than the parent compound, such as 1-amino-2-naphthol [38,39], 1,4-benzoquinone, and 2-naphthol [40].

In a previous study [41], our group studied Ni/Bi-doped SrTiO$_3$ perovskite films on the degradation of AO7 under visible light, with the best results obtained by the Ni/Sr$_{0.9}$Bi$_{0.1}$TiO$_3$ film, in which a relative Abs$_{484 \, nm}$ decay of 83% was achieved after 7 h. These results showed to be promising but restricted to the immobilization technique applied and consequent reduction in surface area. Additionally, studies regarding the influence of experimental parameters on the photocatalytic activity, reusability, and degradation mechanism, were necessary to understand the catalytic behavior of the Bi-doped SrTiO$_3$ perovskites.

In this study, Bi-doped SrTiO$_3$ perovskites (Sr$_{1-x}$Bi$_x$TiO$_3$, x = 0, 0.03, 0.05, 0.07 and 0.1) were synthesized, characterized, and tested as photocatalysts in the degradation of the AO7 dye under visible light. The influence of the amount of doped Bi in the perovskite structure and photocatalytic activity was studied. For the oxide with the best photocatalytic activity, the influence of initial pH, catalyst dose, initial dye concentration, and reusability was assessed, and a possible mechanism is discussed. Acute toxicity assays with *D. magna* were performed to the final solutions. To the best of our knowledge, the influence of Bi-doping of SrTiO$_3$ on the photocatalytic degradation of organic molecules, under visible light, and on toxicity removal has not been reported.

2. Materials and Methods

2.1. Perovskite Powders Preparation and Characterization

The Sr$_{1-x}$Bi$_x$TiO$_3$ (x = 0, 0.03, 0.05, 0.07 and 0.1) perovskite powders were prepared by the solid-state method, in which stoichiometric amounts of SrCO$_3$ (Merk Life Science S.L., Algés, Portugal, ≥99.9%), Bi$_2$O$_3$ (Sigma-Aldrich, Algés, Portugal, ≥99.9%), and TiO$_2$ (Sigma-Aldrich, Algés, Portugal, ≥99.5%) were ground in an agate mortar and heated (tubular furnace Carbolite, model STF, with a Carbonite Gero Type 3216 temperature controller (Sheffield, UK)), at 900 °C (x = 0) or 750 °C (0.03 ≤ x ≤ 0.1) for 24 h. The obtained samples were then reground and reheated at 1200 °C (x = 0) or 750 °C (0.03 ≤ x ≤ 0.1) for 24 h.

X-ray diffractograms (XRD) for all intermediate and final samples were obtained between 2θ = 10 and 90° at a scanning rate of 1.2°/min (Rigaku diffractometer, model DMAX III/C, plus APD Philips v3.5B (Philips, Lisbon, Portugal)) equipped with a monochromatized Cu kα radiation (λ = 0.15406 nm), operating at 40 mA and 30 kW). Results were handled in the Unitcell refinement program [42].

The powder samples' morphological characterization was determined by scanning electron microscopy (SEM) (Hitachi, Tokyo, Japan, model S2700, at 20 keV).

Diffuse reflectance spectra (DRS) were measured with a SPEC STD spectrometer (Sarspec), configured with a 25 μm slit, light source, reflectance probe, and reflectance standard, operating in the ultraviolet–visible range using a Deuterium Tungsten High Power. The bandgap energies were calculated from the diffuse reflectance values through the Kubelka–Munk function (Equation (1)), where R is the diffuse reflectance of the samples, and K and S are the absorption and scattering coefficients, respectively.

$$F(R) = \frac{(1-R)^2}{2R} = \frac{K}{S} \tag{1}$$

The E_g for all samples were determined by extrapolating the linear region of the Tauc plot, with $(F(R).hc/\lambda)^2$ vs. hc/λ, to the abscissa axis, where h is the Planck's constant, c is the speed of light, and λ is the wavelength at the corresponding reflectance.

2.2. Photocatalytic Activity under Visible Light

For the photocatalytic experiments with $Sr_{1-x}Bi_xTiO_3$ (x = 0, 0.03, 0.05, 0.07 and 0.1) samples, 0.002 g or 0.005 g of each powder were dispersed in 10 mL of a 10 mg L^{-1} AO7 (Sigma-Aldrich, Algés, Portugal, 85%) aqueous solution. All suspensions were sonicated for 15 min and stirred in the dark for 45 min, to achieve the adsorption–desorption equilibrium between the dye molecules and the catalyst, after which they were irradiated by visible light (Osram, 300 W (Phillips, Lisbon, Portugal), emission spectrum in Supplementary Materials, Figure S1) for 1 h. For the assays performed with the $Sr_{0.95}Bi_{0.05}TiO_3$, an amount of the powders (0.01, 0.02, and 0.05 g) was dispersed in 100 mL of an aqueous solution of AO7 (10, 25, and 50 mg L^{-1}). The same procedure was followed to achieve the adsorption–desorption equilibrium. The suspensions were irradiated by the same light source for 2 h. For some assays, the pH was adjusted with aqueous solutions of HCl or NaOH. At given intervals, samples of 3 mL were collected and centrifuged, at 5000 rpm for 5 min, and the supernatant was collected. The dye degradation was monitored by UV–visible absorption spectrophotometry (Shimadzu UV-1800 spectrophotometer, Tokyo, Japan), between 200 and 600 nm.

For the optimal experimental conditions, the dye concentration was monitored by reverse-phase high-performance liquid chromatography (RP-HPLC, Shimadzu, Tokyo, Japan), as well as the formation of degradation products, such as sulfanilic acid (SA; Panreac, Applichem, Prior Velho, Portugal, 99.5%), 1-amino-2-naphthol (AN; Sigma-Aldrich, Algés, Portugal, 90%), 1,4-benzoquinone (BQ; Acros Organics, Fisher Scientific, Lisbon, Portugal, 99%), and hydroquinone (HQ; Fluka Analytical, Sigma-Aldrich, Algés, Portugal, ≥99.0%). HPLC analysis was performed in a Shimadzu 20A Prominence HPLC system (DAD-SSPD-M20A; Merck Millipore column, with Purosphere STAR RP-18 endcapped (250 mm × 4 mm (i.d.) and 5 μm particles)). The chromatographic conditions were adapted from previous research [25]. A mixture of 33 mM phosphate buffer (pH 7.0) (KH_2PO_4, Fisher Scientific, Lisbon, Portugal, HPLC grade; K_2HPO_4, AnalaR, 99%) (component A) and acetonitrile (Fisher Chemical, Algés, Portugal, ≥99.99%, HPLC grade) (component B) was used as the eluent, and the elution was performed at 0.7 mL min^{-1}, with a relative percentage of B of 20% for 9 min, increasing to 40% until 11 min, and maintained until 25 min. Detection was carried out at a wavelength of 249 nm for SA, 252 nm for AN, 254 nm for BQ, 288 nm for HQ, and 484 nm for AO7. Carboxylic acids of low molecular weight were detected by ion exclusion chromatography, using the same HPLC apparatus and a Biorad Aminex HPX-87H column (300 mm × 7.8 mm (i.d.)) at 35 °C and at a wavelength of 210 nm for all acids. A 4 mM sulfuric acid aqueous solution was used as eluent, and the elution was performed isocratically at 0.6 mL min^{-1}. All mobile phases and samples were filtered with 0.45 μm and 0.22 μm filters (Whatman, Maidstone, UK), respectively, and the injection volume was 20 μL for both methods.

Acute toxicity assays with *D. magna* were performed using the commercial Daphtoxkit F[TM] Magna Test Kit, following the OECD/OCDE Guideline 202 [43]. The used batch, DM090419, exhibited a mean 24 h EC_{50} for the reference toxicant potassium dichromate of 1.26 mg L^{-1}, which is within the acceptability range of 24 h EC_{50} 0.6–2.1 mg L^{-1} [43]. Standard freshwater, reproducing natural freshwater, was prepared and used in the hatching of the ephippia, prior to toxicity tests, and in the dilution sets for each solution tested. After 2 h and 6 h, solutions resulting from assays that were run under optimal experimental conditions were centrifuged, and the supernatant was filtered with a 0.22 µm filter. From each of these solutions, a set of dilutions (5.625, 11.25, 22.5, 45, and 90%) were prepared with the standard freshwater and poured into four 10 mL wells in the test plate. In each well, 5 neonates (with less than 24 h) were transferred and incubated in the dark for 48 h, at 20 °C. All neonates unable to swim for 15 s, after gentle agitation of the solution, were considered immobilized and registered after 48 h, and the EC_{50} was calculated.

3. Results and Discussion

3.1. Perovskite Powder Characterization

Figure 1 presents the XRD patterns for the $Sr_{1-x}Bi_xTiO_3$ (x = 0, 0.03, 0.05, 0.07 and 0.1) powder perovskites, in which it is possible to identify a predominant well-crystallized phase in all samples, belonging to the cubic perovskite symmetry in a $Pm\bar{3}m$ space group (ICDD file PDF#35-0734). For Bi-doped samples, an extra minority phase was identified as belonging to bismuth titanate, $Bi_4Ti_3O_{12}$ (ICDD file PDF#47-0398), by the presence of its most intense peak, at 29.9° [25].
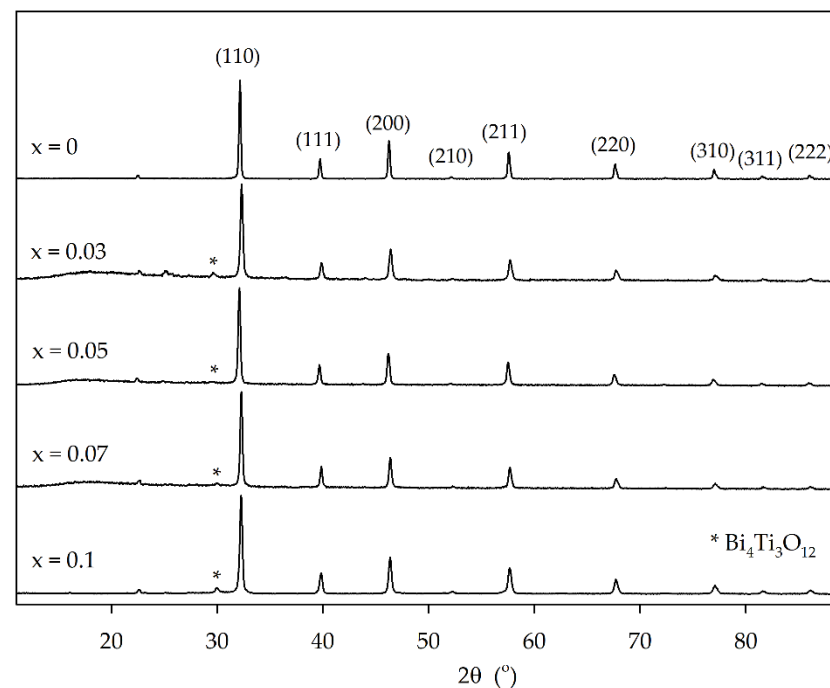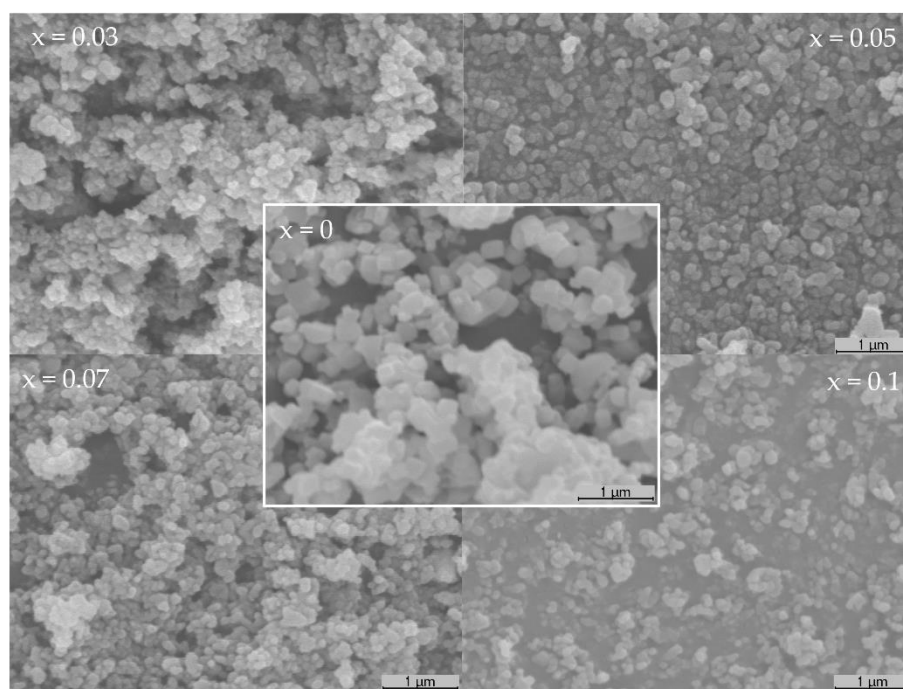

Figure 1. XRD patterns of the $Sr_{1-x}Bi_xTiO_3$ powder samples.

The cell parameters and unit volume, presented in Table 1, vary slightly and in an irregular way with Bi doping, not obeying Végard's law, which is in accordance with the obtained results, as a pure solid solution for the doped samples was not observed. With the substitution of Sr^{2+} cations, with ionic radii of 0.126 nm, by smaller Bi^{3+} cations, with 0.117 nm, the unit cell was expected to contract with the introduction of bismuth in the perovskite structure. However, the cell parameters did not follow this tendency and varied irregularly with Bi content. This corroborates the XRD results, showing that a pure solid solution was not obtained.

Table 1. Cell parameters, unit volume, crystallite size, and bandgap energies for the $Sr_{1-x}Bi_{x}TiO_3$ perovskites.

x	a (nm)	V (nm^3)	Crystallite Size (nm)	E$_g$ (eV)
0	0.39147	0.05999	77.95	3.43
0.03	0.39099	0.05977	59.63	3.66
0.05	0.39187	0.06018	65.87	3.65
0.07	0.39097	0.05976	62.49	3.65
0.1	0.39110	0.05982	53.66	3.66

The crystallite size (Table 1) was calculated by the Scherrer equation, using the full width at half maximum (FWHM) of the (110) peaks, and it is shown to have smaller values for the doped samples. Even though the crystalline size is known to be associated with the smallest particle size in powder form (most likely single crystal), a similar size variation was observed in the SEM images (Figure 2), with a significant reduction in the smaller observed particles when comparing the $SrTiO_3$ to Bi-doped samples.

Figure 2. SEM micrographs of the $Sr_{1-x}Bi_{x}TiO_3$ powder samples (×20,000).

The average observed particle size was smaller for the Bi-doped samples than that for the undoped $SrTiO_3$, with some exhibiting dimensions lower than 100 nm. Regarding the overall morphology, no significant difference was observed.

The calculated E$_g$ values for all samples are presented in Table 1, which increased slightly for the doped samples, from 3.43 eV ($SrTiO_3$) to 3.65–3.66 eV. These values indicate that all oxides are more suitable to be activated by UV light. However, given the identification of a secondary phase in the doped samples, and how it can provide a different layout of the conduction and valence bands [29,44,45], these oxides were tested under visible light.

### 3.2. Photocatalytic Activity under Visible Light

The AO7 dye was used as a model organic pollutant to evaluate the photocatalytic activity of the prepared $Sr_{1-x}Bi_{x}TiO_3$ (x = 0, 0.03, 0.05, 0.07 and 0.1) perovskites. To analyze the dye content during the experiments, the absorbance values at 484 nm were monitored. The band at 484 nm belongs to the visible region of the UV–vis absorption spectrum and results from the conjugated system in the molecule [46]. Before studying the photocatalytic

activity of the oxides, photolysis assays were performed to assess the contribution of the visible light radiation to the degradation of the dye. For an initial AO7 concentration of 10 mg L^{-1}, a 1.0% Abs$_{484 \text{ nm}}$ decrease was observed after 1 h. After 2 h, for all tested AO7 initial concentrations, the relative Abs$_{484 \text{ nm}}$ decay was $\leq$5.8%. Adsorption assays were also performed (data not shown) for all tested oxides, to determine the time necessary to achieve the adsorption–desorption equilibrium between the dye and the catalyst. After 1 h, the amounts of adsorbed AO7 were $\leq$7.0% and $\leq$8.6%, for a catalyst dose of 0.2 and 0.5 g L^{-1}, respectively.

The effects of Bi doping on the photocatalytic activity of the perovskites under visible light were tested, and the results are presented in Figure 3a. The results show a poor relative absorbance decay for the strontium titanate sample, with 3.7% and 5.3% removals after 1 h irradiation for catalyst doses of 0.2 g L^{-1} and 0.5 g L^{-1}, respectively. These values are in accordance with the calculated E$_g$ value of 3.43 eV, which indicates that SrTiO$_3$ would be more suitable to be activated by UV light. However, despite the similar high E$_g$ values (3.65–3.66 eV), the Bi-doped samples exhibited a significant increase in the photocatalytic activity, when compared with the undoped SrTiO$_3$, with relative Abs$_{484 \text{ nm}}$ decays above 97.5% after 1 h, for both Sr$_{0.95}$Bi$_{0.05}$TiO$_3$ and Sr$_{0.93}$Bi$_{0.07}$TiO$_3$ samples. This behavior could be due to the occurrence of the Bi$_4$Ti$_3$O$_{12}$ secondary phase in all doped samples, alongside the Sr$_{1-x}$Bi$_x$TiO$_3$ cubic perovskite phase, resulting in a synergetic effect between both phases, given that the Bi$_4$Ti$_3$O$_{12}$ possess photocatalytic activity, achieving a relative Abs$_{484 \text{ nm}}$ decrease of 27.6% after 2 h, for a catalyst dose of 0.2 g L^{-1}, and under the same conditions (Supplementary Material Figure S2). Another possibility is the formation of a heterostructure, where the valence and conduction bands are distributed in such a manner that the recombination of photogenerated electron–hole pair could be reduced, increasing the photocatalytic activity of the samples with that structure [29,44,45]. However, given the available results, the latter cannot be confirmed. Further studies about the band structures and work function of the heterostructures need to be performed [47,48]. This effect in the catalytic activity for the degradation of AO7 (Figure 3a) increases significantly with the amount of doped bismuth until x = 0.1, where a decrease in the relative Abs$_{484 \text{ nm}}$ decay is observed, indicating that there is an optimal ratio between both phases. The smaller particle size, observed for the doped samples (Figure 2), should also be considered, as it results in a higher surface area for the catalytic reaction to occur.

Given that the best results were obtained for the Sr$_{0.95}$Bi$_{0.05}$TiO$_3$ perovskite, further studies were performed with this sample to infer the optimal experimental conditions for the AO7 photocatalytic degradation. Figure 3b shows the influence of the catalyst dosage in the degradation of 25 mg L^{-1} AO7 aqueous solutions. An increase in the initial catalyst dose from 0.1 g L^{-1} to 0.2 g L^{-1} resulted in an improvement in the decolorization rate throughout the 2 h assay, with observed Abs$_{484 \text{ nm}}$ decays increasing from 83.7% to 95.8% after 2 h. However, no improvement was observed with the increase in the powder concentration from 0.2 g L^{-1} to 0.5 g L^{-1}. An initial increase in the catalyst concentration led to a higher decolorization rate, which could be associated with an increase in the available catalyst surface area, followed by no perceivable improvement for the highest tested concentration. This behavior could be due to the increase in the turbidity of the perovskite suspension, hindering the penetration of the visible light radiation and catalyst activation.

Regarding the influence of the initial dye concentration (Figure 3c), the relative Abs$_{484 \text{ nm}}$ decay decreased with the increase in the initial AO7 concentration from 98.9% to 57.5% after 2 h, for 10 mg L^{-1} to 50 mg L^{-1}, respectively. When analyzing the amount of removed dye (mg of removed AO7 per gram of catalyst, Figure 3c inset), it is possible to observe that the value increased with the initial increase in dye concentration (from 45 to, approximately, 100 mg of AO7 removed per g of catalyst), followed by no significant variation for the highest dye concentration. This behavior could be explained by a higher concentration of AO7 molecules adsorbed at the available catalyst surface area for the 50 mg L^{-1} AO7 assay, delaying the degradation mechanism and leading to results similar to those obtained at a lower concentration of 25 mg L^{-1} [49].
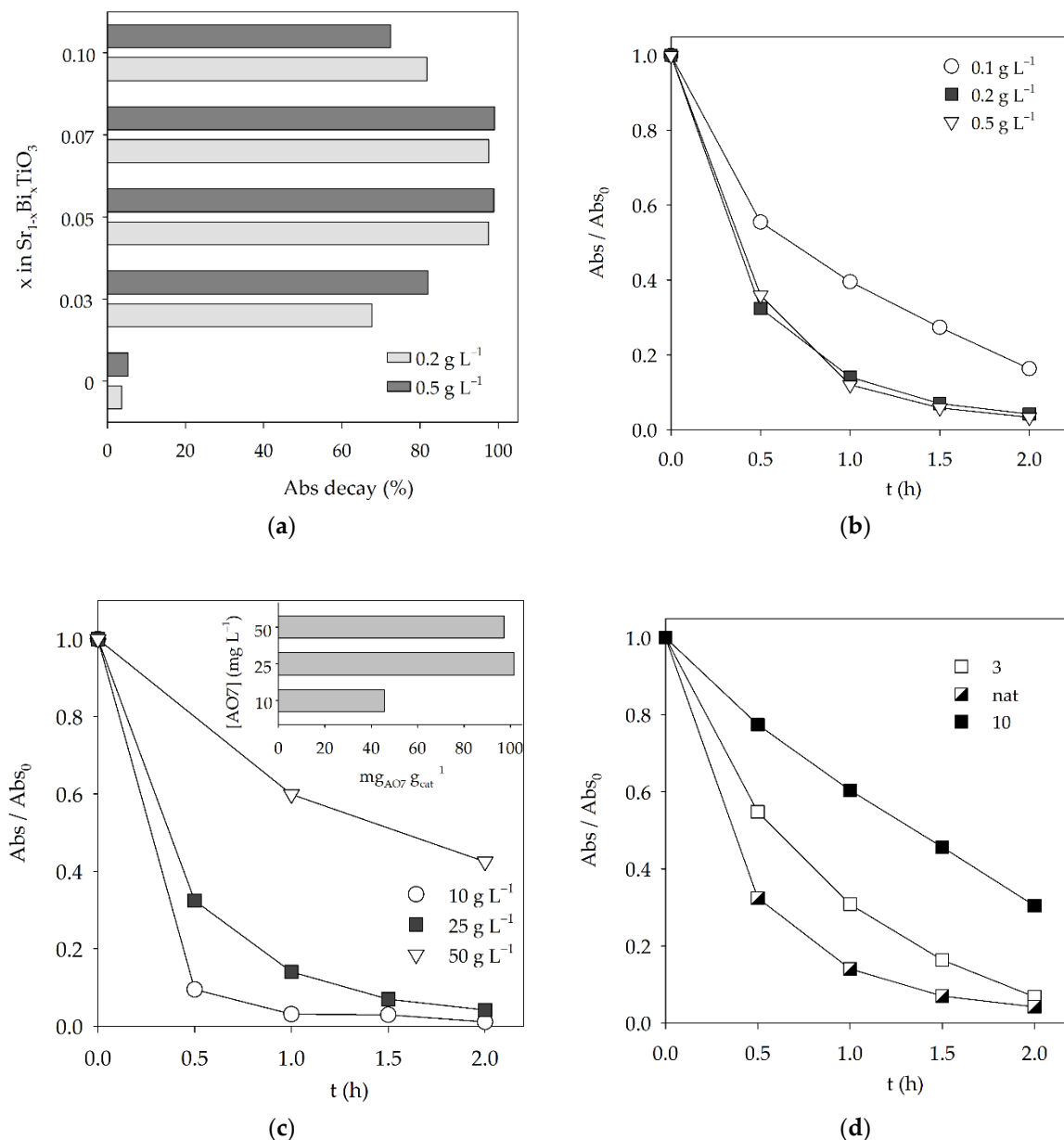
Figure 3. Influence of (**a**) Bi doping on the relative $Abs_{484\,nm}$ decay after 1 h (C_i AO7 = 10 mg L^{-1}, at two catalyst doses); (**b**) catalyst dose; (**c**) initial dye concentration (inset mg AO7 removed/g of catalyst, for the tested dye concentrations); (**d**) pH on the relative absorbance decays, measured at 484 nm, for the photocatalytic degradation of AO7, with the $Sr_{0.95}Bi_{0.05}TiO_3$ perovskite under visible light.

It is known that the pH can influence the interaction between the dye molecules and the catalyst, as it can affect the catalyst surface and dye molecule charge, and subsequent AO7 adsorption [49]. As it can be seen in Figure 3d, the best results were obtained at the naturally occurring pH (~6) of the suspension, indicating that this pH value is ideal for the dye degradation mechanism to occur, as it could promote an ideal adsorption rate and subsequent photocatalytic reaction. It could also be related to the pH of the zero-point charge of the $Sr_{0.95}Bi_{0.05}TiO_3$ catalyst.

Reusability is an important parameter to take into consideration when testing a catalyst. To evaluate this characteristic, the perovskite was recovered after the photocatalytic experiment, washed with distilled water, and air-dried before being reused in the degradation of 10 mg L^{-1} AO7, using 0.2 g L^{-1} catalyst and without controlling the pH. The

recovery percentage of the catalyst was between 78.2% and 80.2%. This percentage could be improved by using filters or membranes to facilitate the separation. However, this would increase the cost of the overall process. Results showed no significant loss in photocatalytic activity (Figure 4). Moreover, XRD and DRS analysis were performed on the used catalyst (Supplementary Material Figures S3–S5, respectively), with no significant alteration of the perovskite structure and cell parameters and calculated E_g values (3.65 eV). This shows that the $Sr_{0.95}Bi_{0.05}TiO_3$ can be reused without significant loss of either photocatalytic activity under visible light or structural, morphological, and optical stability.
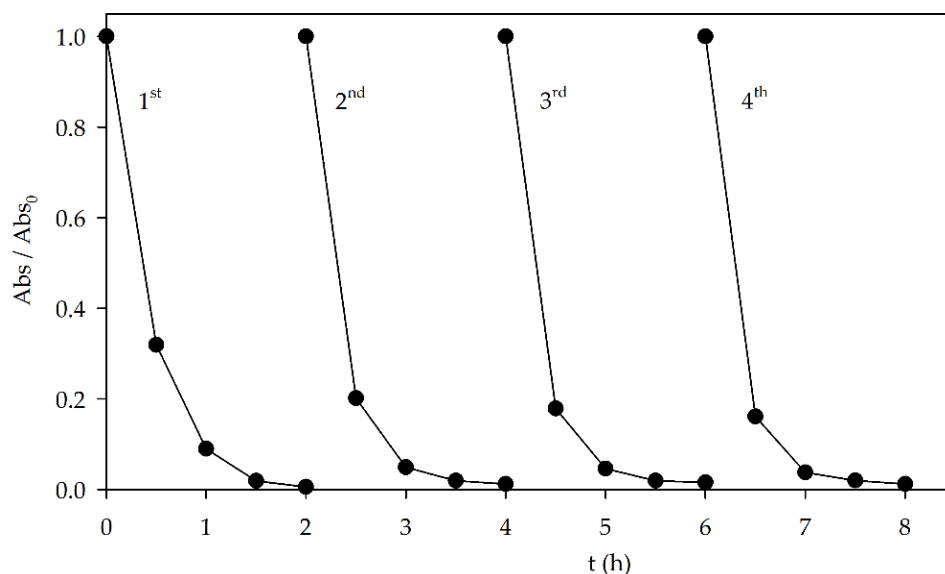
Figure 4. Reusability of the $Sr_{0.95}Bi_{0.05}TiO_3$ catalyst (0.2 g L^{-1}) on the photocatalytic degradation of AO7 (10 mg L^{-1}) under visible light, during four cycles.

*3.3. Analysis of the Degradation Products and Proposed Mechanism*

Experiments carried out with $Sr_{0.95}Bi_{0.05}TiO_3$ under optimal conditions and AO7 concentrations of 10 and 25 mg L^{-1} were performed for 6 h and monitored by RP-HPLC, to assess the dye concentration decay and detect some of the possible degradation by-products such as SA, AN, (previously detected and reported [25,50]) BQ, HQ, and some low-molecular-weight carboxylic acids (Figure 5).

The AO7 concentration decay was observed to occur primarily during the first and third hours of the experiments for initial dye concentrations of 10 mg L^{-1} and 25 mg L^{-1}, respectively. SA and AN were detected during these times, with an increase in concentration until reaching a maximum value, followed by a decrease until the end of both assays. In the case of the experiment conducted with an initial dye concentration of 10 mg L^{-1}, both metabolites were completely degraded after 3 h, which coincided with the formation and detection of some low-molecular-weight acids such as maleic and acetic acid (Figure 5). Formic acid was also detected but in very low concentration. Similar behavior was observed for the assays performed at 25 mg L^{-1}, with the slower formation and degradation times for all detected metabolites. BQ and HQ were also detected under both experimental conditions, both presenting similar outline profiles as SA.

This behavior shows that once the dye concentration is low enough, and diffusion is the main controlling step, the metabolites begin to suffer photocatalytic degradation as well, and in some instances, full degradation is achieved.

By analyzing the order of detection and overall outline of all monitored compounds, some insights were inferred, based on which a simple degradation mechanism is proposed in Figure 6.
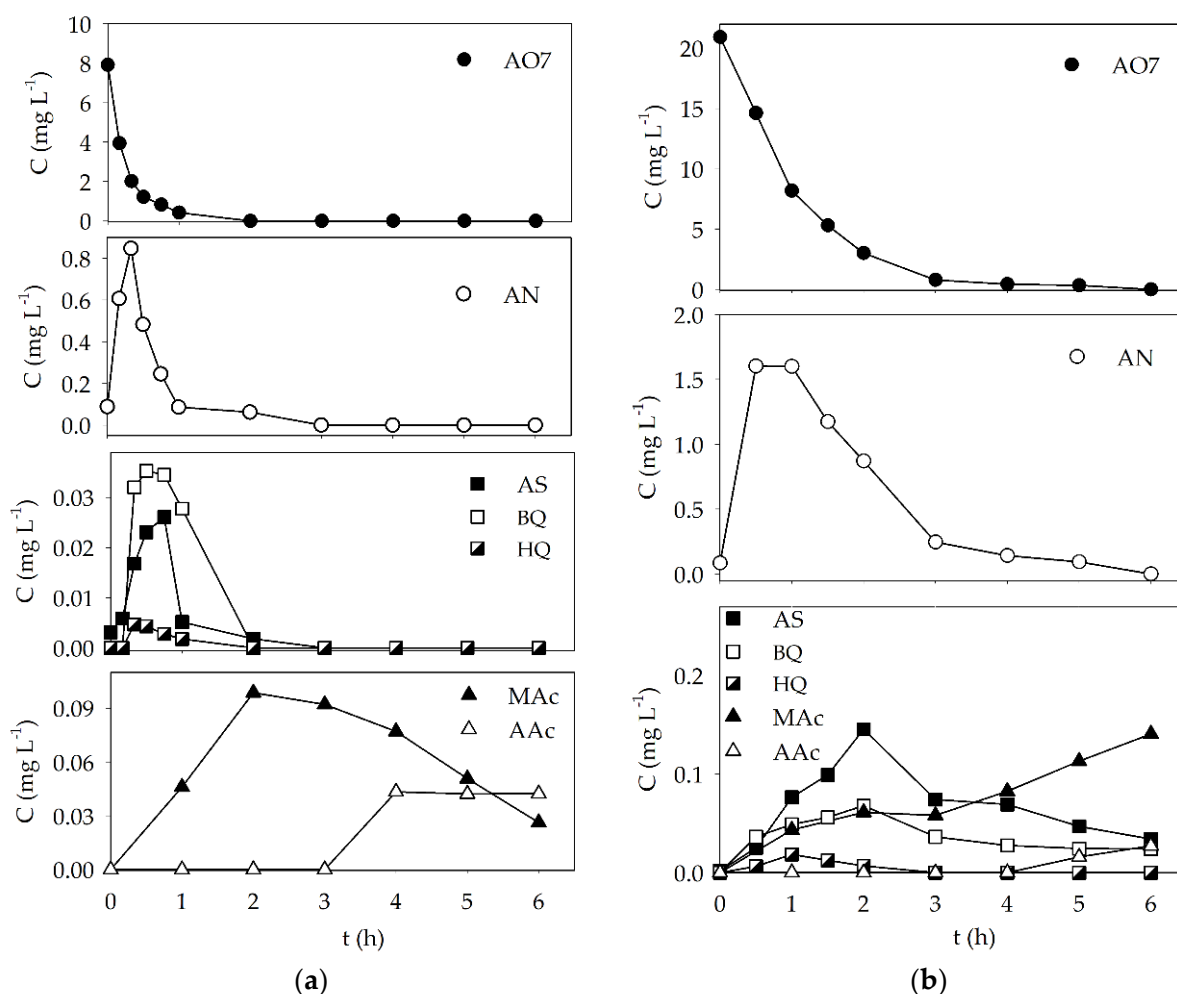
Figure 5. Concentration variation for the AO7 dye and some degradation products during the photocatalytic degradation of (**a**) 10 mg L^{-1} and (**b**) 25 mg L^{-1} of AO7 under visible light with Sr$_{0.95}$Bi$_{0.05}$TiO$_3$ perovskite (0.2 g L^{-1}).

In this proposed mechanism, it was assumed that the cleavage of the azo bond is the most likely first step in the degradation pathway [51], which is corroborated by the detection of the main reaction products AN and SA, formed shortly after the degradation assays started and AO7 concentration began to decrease. SA could suffer further oxidation into other detected benzenic compounds such as HQ and BQ, which, as previously mentioned, had similar outlines as SA. The same could occur with AN, which, initially, led to the formation of other naphthalenic compounds. The formation of low-molecular-weight acids follows the opening of benzenic and naphtalenic rings and further oxidation reactions, and it occurs after a significant concentration of the preceding high-molecular-weight metabolites is already decreasing. Ideally, the degradation pathway leads to the total mineralization of the molecules into CO_2, H_2O, and other inorganic substances.

TOC values were determined for both assays, after 2 and 6 h, with results presented in Table 2. Good mineralization was observed after 6 h for the assay with 10 mg L^{-1}, with 42.3% TOC removal, which could indicate that with enough time, almost complete mineralization could be achieved. For the assay at 25 mg L^{-1}, the low TOC removals (14.4% and 19.4% after 2 h and 6 h, respectively) are in accordance with the detection of several metabolites at both times.
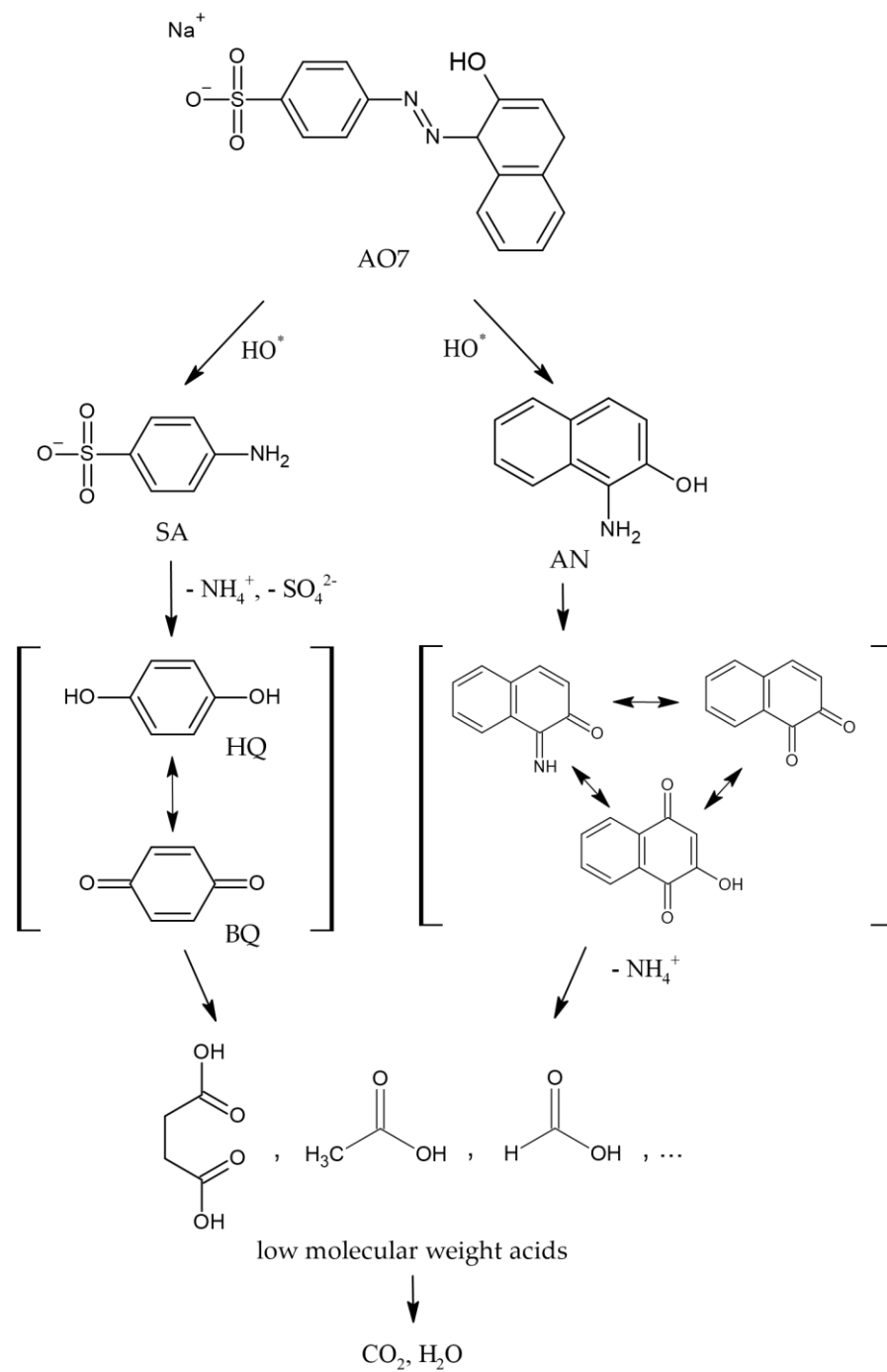
Figure 6. Proposed AO7 degradation pathway.

Table 2. TOC removals (%) for the photocatalytic degradation of AO7 with $Sr_{0.95}Bi_{0.05}TiO_3$ perovskite (0.2 g L^{-1}) under visible light.

AO7 Initial Concentration (mg L^{-1})	TOC Removal (%)	
	2 h	6 h
10	11.6	42.3
25	14.4	19.4

3.4. Kinetics

As it can be seen in Figure 5, the dye concentration decreased exponentially with the irradiation time, meaning that it can be described by a pseudo-first-order rate model. The apparent rate constant (k) can be calculated as $\ln(C_0/C) = kt$, where C is AO7 concentration and t irradiation time (Figure 7) and are $3.2\,h^{-1}$ and $1.0\,h^{-1}$ for the experiments conducted with $10\,mg\,L^{-1}$ and $25\,mg\,L^{-1}$, respectively. The AO7 degradation rate decreased with the increase in dye concentration not simply because of the relative amount of dye molecules and available catalyst surface area, but due to the formation of higher concentrations of degradation products for the assay with $25\,mg\,L^{-1}$, which will also adsorb on the catalyst surface, slowing the AO7 degradation mechanism.
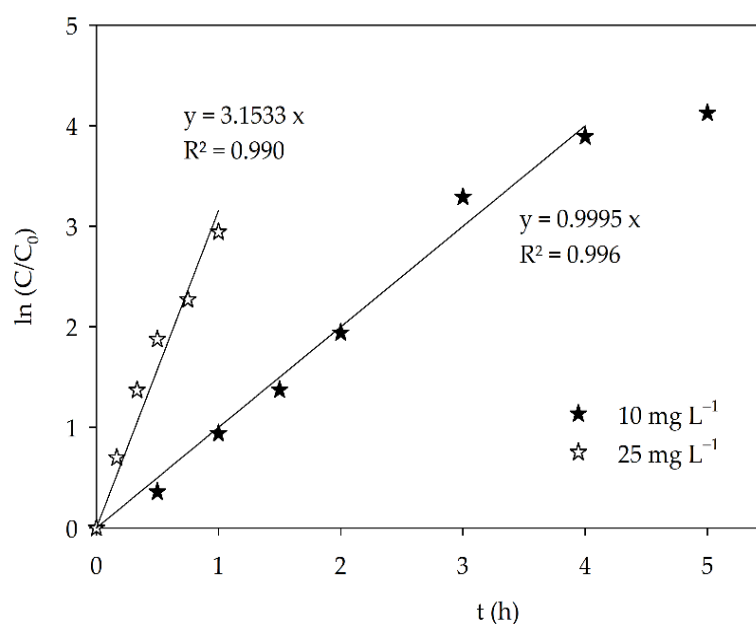
Figure 7. Pseudo-first-order kinetics for AO7 degradation under visible light over $Sr_{0.95}Bi_{0.05}TiO_3$.

For the AO7 initial concentration of $25\,mg\,L^{-1}$, it is possible to see that the mentioned apparent rate constant was calculated for the first 4 h, followed by a visible decrease in the slope for the final hour of the assay. This is in accordance with the detection of several by-products during the photocatalytic assay, and their degradation and/or counter diffusion occurring in a way that, for some of the compounds, total degradation was also observed.

3.5. Toxicity

Both initial solutions were below the dye EC_{50} (*D. magna*) of $57.26\,mg\,L^{-1}$. However, given the fact that some metabolites can be significantly more toxic than the parent compound, it is extremely important to monitor the toxicity of the final solutions to evaluate if the photocatalyst used is efficient enough to produce non-toxic final solutions.

For the ecotoxicity evaluation, acute toxicity (immobilization) assays with *D. magna* were performed for the solutions obtained after 2 and 6 h, for both initial dye concentrations. The EC_{50} was assessed by performing the acute immobilization test on a set of dilutions of each solution. The obtained result is expressed in concentration (%) of the initial solution, estimated to immobilize 50% of the *D. magna* within 48 h. The assay performed with $10\,mg\,L^{-1}$ AO7, for both samples after 2 and 6 h, showed no toxicity to the tested organism. These results are in accordance with the detection of only small carboxylic acids at both 2 h (maleic acid) and 6 h (maleic, acetic, and formic acid), which are known to have very low toxicity (EC_{50} (*D. magna*) $\geq 48.81\,mg\,L^{-1}$). However, for the assay with $25\,mg\,L^{-1}$ AO7, after 2 h, an EC_{50} value of 61.21% was obtained. This could be explained by the presence of AN in a concentration of $0.87\,mg\,L^{-1}$ in the 2 h sample, which is known to be a very

toxic compound [38,39], with a 48 h EC_{50} (*D. magna*) value of 0.37 mg L^{-1}. Nevertheless, as this metabolite suffered complete degradation until the end of the photocatalytic assay, the final solution (6 h) showed no toxicity to *D. magna*. These results show that the application of $Sr_{0.95}Bi_{0.05}TiO_3$ as a photocatalyst in the degradation of the AO7 dye with visible light is efficient enough to also degrade the toxic metabolites successfully, producing final solutions non-toxic to *D. magna*.

The $Sr_{0.95}Bi_{0.05}TiO_3$ oxide showed significant photocatalytic activity for the degradation of the AO7 dye under visible light, when compared with other metal oxide catalysts (Table 3).

Table 3. Comparing the photocatalytic activity of different photocatalysts on the degradation of aqueous solutions of AO7 under visible light radiation.

Photocatalyst	Catalyst Dose (g L^{-1})	C_i AO7 (mg L^{-1})	t (min)	Degradation Efficiency (%)	Ref.
7% Co doped CeO NPs	1.0	15	180	95.4	[52]
NiO NPs	1.0	10	160	90.2	[53]
$AuPt/Bi_2O_3$	0.5	5	60	~98	[54]
$Fe(2.5)-TiO_2$	3	10	180	~90	[55]
$BaFeO_3$	0.5	5	360	97	[56]
$Ni/Sr_{0.9}Bi_{0.1}TiO_3$	NA	25	420	83	[41]
$Sr_{0.95}Bi_{0.05}TiO_3$	0.2	10	180	98.9	[This work]

4. Conclusions

Bi-doped $SrTiO_3$ perovskite ($Sr_{1-x}Bi_xTiO_3$, x = 0, 0.03, 0.05, 0.07 and 0.1) powders were synthesized and applied as photocatalysts in the degradation of AO7 solutions under visible light. All doped samples exhibited a significant improvement in their photocatalytic activity when compared with the undoped $SrTiO_3$. This improvement can be associated with the presence of a secondary phase, $Bi_4Ti_3O_{12}$, and a possible synergistic effect between both phases. The possible formation of a heterostructure was also theorized, but further studies need to be performed. The best results were obtained with the $Sr_{0.95}Bi_{0.05}TiO_3$ perovskite (0.2 g L^{-1}), achieving complete AO7 degradation after 2 h and 3 h, for initial dye concentration of 10 mg L^{-1} and 25 mg L^{-1}, respectively, at natural pH and under visible light. The ecotoxicity of the solutions was evaluated through acute toxicity assays with *D. magna*, and the solutions were found to be non-toxic after 2 h and 6 h for the initial dye concentrations of 10 mg L^{-1} and 25 mg L^{-1}, respectively.

Author Contributions: Conceptualization, A.L. and L.C.; data curation, M.J.N. and L.C.; formal analysis, M.J.N., A.L. and L.C.; investigation, M.J.N.; methodology, M.J.N.; project administration, A.L.; resources, M.J.P.; supervision, A.L. and L.C.; validation, M.J.N. and M.J.P.; visualization, M.J.N., A.L. and L.C.; writing—original draft, M.J.N.; writing—review and editing, A.L., M.J.P. and L.C. All authors have read and agreed to the published version of the manuscript.

Institutional Review Board Statement: Not applicable.

Informed Consent Statement: Not applicable.

Data Availability Statement: Not applicable.

Conflicts of Interest: The authors declare no conflict of interest. The funders had no role in the design of the study; in the collection, analyses, or interpretation of data; in the writing of the manuscript; in the decision to publish the results.

References

1. Khataee, A.R.; Pons, M.N.; Zahraa, O. Photocatalytic degradation of three azo dyes using immobilized TiO_2 nanoparticles on glass plates activated by UV light irradiation: Influence of dye molecular structure. *J. Hazard. Mater.* **2009**, *168*, 451–457. [CrossRef] [PubMed]

2. Bansal, P.; Singh, D.; Sud, D. Photocatalytic degradation of azo dye in aqueous TiO_2 suspension: Reaction pathway and identification of intermediates products by LC/MS. *Sep. Purif. Technol.* **2010**, *72*, 357–365. [CrossRef]

3. Jaimes-Ramírez, R.; Vergara-Sánchez, J.; Silva-Martínez, S. Solar assisted degradation of acid orange 7 textile dye in aqueous solutions by Ce-doped TiO_2. *Mex. J. Sci. Res.* **2012**, *1*, 42–55.

4. Posa, V.R.; Annavaram, V.; Somala, A.R. Fabrication of graphene–TiO_2 nanocomposite with improved photocatalytic degradation for acid orange 7 dye under solar light irradiation. *Bull. Mater. Sci.* **2016**, *39*, 759–767. [CrossRef]

5. Ozmen, N.; Erdemoglu, S.; Gungordu, A.; Asilturk, M.; Turhan, D.O.; Akgeyik, E.; Harper, S.L.; Ozmen, M. Photocatalytic degradation of azo dye using core@shell nano-TiO_2 particles to reduce toxicity. *Environ. Sci. Pollut. Res. Int.* **2018**, *25*, 29493–29504. [CrossRef]

6. Rohilla, S.; Gupta, A.; Kumar, V.; Kumari, S.; Petru, M.; Amor, N.; Noman, M.T.; Dalal, J. Excellent UV-light triggered photocatalytic performance of $ZnO.SiO_2$ nanocomposite for water pollutant compound methyl orange dye. *Nanomaterials* **2021**, *11*, 2548. [CrossRef]

7. Rani, S.; Naresh, G.; Mandal, T.K. Coupled-substituted double-layer Aurivillius niobates: Structures, magnetism and solar photocatalysis. *Dalton Trans.* **2020**, *49*, 1433–1445. [CrossRef]

8. The European Parllament and the Council of the European -Union, Regulation (EU) 2020/741 of the European parliament and of the council of 25 May 2020 on minimum requirements for water reuse. *Off. J. Eur. Union* **2020**, *63*, 32–55. Available online: https://eur-lex.europa.eu/legal-content/EN/TXT/PDF/?uri=CELEX:32020R0741&from=EN (accessed on 7 June 2021).

9. Xu, Y.; Yang, M.; Chen, B.; Wang, X.; Chen, H.; Kuang, D.; Su, C. A $CsPbBr_3$ perovskite quantum dot/graphene oxide composite for photocatalytic CO_2 reduction. *J. Am. Chem. Soc.* **2017**, *139*, 5660–5663. [CrossRef]

10. Zhu, Y.; Liu, Y.; Miller, K.A.; Zhu, H.; Egap, E. Lead halide perovskite nanocrystals as photocatalysts for PET-RAFT polymerization under visible and near-infrared irradiation. *ACS Macro Lett.* **2020**, *9*, 725–730. [CrossRef]

11. Soltani, T.; Entezari, M.H. Sono-synthesis of bismuth ferrite nanoparticles with high photocatalytic activity in degradation of Rhodamine B under solar light irradiation. *Chem. Eng. J.* **2013**, *223*, 145–154. [CrossRef]

12. Tummino, M.L.; Laurenti, E.; Deganello, F.; Prevot, A.B.; Magnacca, G. Revisiting the catalytic activity of a doped $SrFeO_3$ for water pollutants removal: Effect of light and temperature. *Appl. Catal. B Environ.* **2017**, *207*, 174–181. [CrossRef]

13. Dhiman, T.K.; Singh, S. Enhanced catalytic and photocatalytic degradation of organic pollutant Rhodamine-B by $LaMnO_3$ nanoparticles synthesized by non-aqueous sol-gel route. *Phys. Status Solidi A* **2019**, *216*, 1900012. [CrossRef]

14. Ismael, M.; Wark, M. Perovskite-type $LaFeO_3$: Photoelectrochemical properties and photocatalytic degradation of organic pollutants under visible light irradiation. *Catalysts* **2019**, *9*, 342. [CrossRef]

15. Haruna, A.; Abdulkadir, I.; Idris, S.O. Photocatalytic activity and doping effects of $BiFeO_3$ nanoparticles in model organic dyes. *Heliyon* **2020**, *6*, e03237. [CrossRef]

16. Jana, R.; Gupta, A.; Choudhary, R.; Pandey, O.P. Influence of cationic doping at different sites in $NaNbO_3$ on the photocatalytic degradation of methylene blue dye. *J. Sol-Gel Sci. Technol.* **2020**, *96*, 405–415. [CrossRef]

17. Safari, S.; Ahmadian, S.M.S.; Amani-Ghadim, A.R. Visible light photocatalytic activity enhancing of $MTiO_3$ perovskites by M cation (M = Co, Cu, and Ni) substitution and Gadolinium doping. *J. Photochem. Photobiol. A Chem.* **2020**, *394*, 112461. [CrossRef]

18. Dara, M.; Hassanpour, M.; Amiri, O.; Baladi, M.; Salvati-Niasari, M. Sol-gel auto combustion synthesis, characterization, and application of Tb_2FeMnO_6 nanostructures as an effective photocatalyst for the discoloration of organic contaminants in wastewater. *RSC Adv.* **2022**, *11*, 26844. [CrossRef]

19. Fernandes, D.; Raubach, C.W.; Jardim, P.L.G.; Cava, S.S. Synthesis of $NaNbO_3$ nanowires and their photocatalytic activity. *Ceram. Int.* **2021**, *47*, 10185–10188. [CrossRef]

20. Ghafoor, A.; Bibi, I.; Majid, F.; Kamal, S.; Ata, S.; Nazar, N.; Iqbal, M.; Raza, M.A.S.; Almoneef, M.M. Ce and Fe doped $LaNiO_3$ synthesized by micro-emulsion route. Effect of doping on visible light adsorption for photocatalytic application. *Mater. Res. Express* **2021**, *8*, 085009. [CrossRef]

21. Paul, D.; Das, G. Efficient solid-state synthesis of biomineralized vaterite-derived pure $CaMnO_3$ perovskite for effective photocatalysis. *CrystEngComm* **2021**, *23*, 4050. [CrossRef]

22. Petrović, S.; Rožić, L.; Grbić, B.; Radić, N.; Cherkezova-Zheleva, Z.; Stojadinović, S. Structural, optical and photocatalytic properties of $LaTi_{0.4}Mg_{0.4}Fe_{0.2}O_3$ perovskite prepared by high-energy ball milling. *J. Solid State Chem.* **2021**, *297*, 122085. [CrossRef]

23. Prashanth, K.S.; Raghu, M.S.; Alharthi, F.A.; Sreenivasa, S.; Devi, V.S.A.; Krishnaiah, P.; Rajamma, D.B.; Akshatha, S.; Jeon, B.H.; Parashuran, L. Solar light sensitive hybrid $Ce^{4+/3+}$ doped perovskite magnesium zirconate nano cubes for photocatalytic hydrogen evolution and organic pollutant degradation in water. *J. Environ. Chem. Eng.* **2021**, *9*, 105364. [CrossRef]

24. Chen, L.; Zhang, S.; Wang, L.; Xue, D.; Yin, S. Preparation and photocatalytic properties of strontium titanate powders via sol–gel process. *J. Cryst. Growth* **2009**, *311*, 746–748. [CrossRef]

25. Nunes, M.J.; Lopes, A.; Pacheco, M.J.; Ciríaco, L. Preparation, characterization and environmental applications of $Sr_{1-x}(La,Bi)_xTiO_3$ perovskites immobilized on Ni-foam: Photodegradation of the Acid Orange 7. *Environ. Sci. Pollut. Res.* **2017**, *24*, 11102–11110. [CrossRef]

26. Li, F.; Yu, K.; Lou, L.; Su, Z.; Liu, S. Theoretical and experimental study of La/Ni co-doped $SrTiO_3$ photocatalyst. *Mater. Sci. Eng. B* **2010**, *172*, 136–141. [CrossRef]

27. Jia, A.; Su, Z.; Lou, L.; Liu, S. Synthesis and characterization of highly-active nickel and lanthanum co-doped $SrTiO_3$. *Solid State Sci.* **2010**, *12*, 1140–1145. [CrossRef]

28. Ghaffari, M.; Tan, P.Y.; Oruc, M.E.; Tan, O.K.; Tse, M.S.; Shannon, M. Effect of ball milling on the characteristics of nano structure $SrFeO_3$ powder for photocatalytic degradation of methylene blue under visible light irradiation and its reaction kinetics. *Catal. Today* **2011**, *161*, 70–77. [CrossRef]

29. Wang, W.; Tade, M.O.; Shao, Z.P. Research progress of perovskite materials in photocatalysis- and photovoltaics-related energy conversion and environmental treatment. *Chem. Soc. Rev.* **2015**, *44*, 5371–5408. [CrossRef]

30. Hou, D.; Hu, X.; Ho, W.; Hu, P.; Huang, Y. Facile fabrication of porous Cr-doped $SrTiO_3$ nanotubes by electrospinning and their enhanced visible-light-driven photocatalytic properties. *J. Mater. Chem. A* **2015**, *3*, 3935–3943. [CrossRef]

31. Liu, J.W.; Chen, G.; Li, Z.H.; Zhang, Z.G. Electronic structure and visible light photocatalysis water splitting property of chromium-doped $SrTiO_3$. *J. Solid State Chem.* **2006**, *179*, 3704–3708. [CrossRef]

32. Wu, G.; Li, P.; Xu, D.; Luo, B.; Hong, Y.; Shi, W.; Liu, C. Hydrothermal synthesis and visible-light-driven photocatalytic degradation for tetracycline of Mn-doped $SrTiO_3$ nanocubes. *Appl. Surf. Sci.* **2015**, *333*, 39–47. [CrossRef]

33. Jamil, T.S.; Abbas, H.A.; Youssief, A.M.; Mansor, E.S.; Hammad, F.F. The synthesis of nano-sized undoped, Bi doped and Bi, Cu co-doped $SrTiO_3$ using two sol–gel methods to enhance the photocatalytic performance for the degradation of dibutyl phthalate under visible light. *Comptes Rendus Chim.* **2017**, *20*, 97–106. [CrossRef]

34. Garcia, C.R.; Oliva, J.; Chávez, D.; Esquivel, B.; Gómez-Solís, C.; Martínez-Sánchez, E.; Mtz-Enriquez, A.I. Effect of Bismuth Dopant on the Photocatalytic Properties of $SrTiO_3$ under Solar Irradiation. *Top. Catal.* **2020**, *64*, 155–166. [CrossRef]

35. Brillas, E.; Martínez-Huitle, C.A. Decontamination of wastewaters containing synthetic organic dyes by electrochemical methods. An updated review. *Appl. Catal. B Environ.* **2015**, *166–167*, 603–643. [CrossRef]

36. Rawat, D.; Mishra, V.; Sharma, R.S. Detoxification of azo dyes in the context of environmental processes. *Chemosphere* **2016**, *155*, 591–605. [CrossRef]

37. Martínez-Huitle, C.A.; Brillas, E. Decontamination of wastewaters containing synthetic organic dyes by electrochemical methods: A general review. *Appl. Catal. B Environ.* **2009**, *87*, 105–145. [CrossRef]

38. Gottlieb, A.; Shaw, C.; Smith, A.; Wheatley, A.; Forsythe, S. The toxicity of textile reactive azo dyes after hydrolysis and decolourisation. *J. Biotechnol.* **2003**, *101*, 49–56. [CrossRef]

39. Rawat, D.; Sharma, R.S.; Karmakar, S.; Arora, L.S.; Mishra, V. Ecotoxic potential of a presumably non-toxic azo dye. *Ecotoxicol. Environ. Saf.* **2018**, *148*, 528–537. [CrossRef]

40. Le, T.X.H.; Nguyen, T.V.; Yacouba, Z.A.; Zoungrana, L.; Avril, F.; Petit, E.; Mendret, J.; Bonniol, V.; Bechelany, M.; Lacour, S.; et al. Toxicity removal assessments related to degradation pathways of azo dyes: Toward an optimization of Electro-Fenton treatment. *Chemosphere* **2016**, *161*, 308–318. [CrossRef]

41. Nunes, M.J.; Lopes, A.; Pacheco, M.J.; Ciríaco, L.; Fiadeiro, P.T. Photocatalytic degradation of the AO7 under visible light with Bi-doped SrTiO3. In *Textiles, Identity and Innovation: In Touch*; CRC Press: London, UK, 2020; pp. 349–355. [CrossRef]

42. Holland, T.J.B.; Redfern, S.A.T. *Unitcell*; Computer Program Developed at the University of Cambridge; University of Cambridge: Cambridge, UK, 1995.

43. OCDE. *Test No. 202: Daphnia sp. Acute Immobilisation Test, OECD Guidelines for testing of Chemicals, Section 2*; OECD Publishing: Paris, France, 2004.

44. Zhao, W.; Wang, H.; Feng, X.; Jiang, W.; Zhao, D.; Li, J. Hydrothermal synthesis and photocatalytic activities of $Bi_4Ti_3O_{12}/SrTiO_3$ composite micro-platelets. *Mater Res. Bull.* **2015**, *70*, 179–183. [CrossRef]

45. Che, H.; Chen, J.; Huang, K.; Hu, W.; Hu, H.; Liu, X.; Che, G.; Liu, C.; Shi, W. Construction of $SrTiO_3/Bi_2O_3$ heterojunction towards to improved separation efficiency of charge carriers and photocatalytic activity under visible light. *J. Alloys Compd.* **2016**, *688*, 882–890. [CrossRef]

46. Stylidi, M.; Kondarides, D.I.; Verykios, X.E. Visible light-induced photocatalytic degradation of Acid Orange 7 in aqueous TiO_2 suspensions. *Appl. Catal. B Environ.* **2004**, *47*, 189–201. [CrossRef]

47. Zhu, Y.; Liu, Y.; Ai, Q.; Gao, G.; Yuan, L.; Fang, Q.; Tian, X.; Zhang, X.; Egap, E.; Ajayan, P.M.; et al. In situ synthesis of lead-free halide perovskite–COF nanocomposites as photocatalysts for photoinduced polymerization in both organic and aqueous phases. *ACS Mater. Lett.* **2022**, *4*, 464–471. [CrossRef]

48. Wang, Y.; Hu, Z.; Wang, W.; He, H.; Deng, L.; Zhang, Y.; Huang, J.; Zhao, N.; Yu, G.; Liu, Y. Design of well-defined shell–core covalent organic frameworks/metal sulfide as an efficient Z-scheme heterojunction for photocatalytic water splitting. *Chem. Sci.* **2021**, *12*, 16065. [CrossRef] [PubMed]

49. Muthirulan, P.; Devi, C.N.; Sundaram, M.M. A green approach to the fabrication of titania–graphene nanocomposites: Insights relevant to efficient photodegradation of Acid Orange 7 dye under solar irradiation. *Mater. Sci. Semicond. Process.* **2014**, *25*, 219–230. [CrossRef]

50. Carvalho, C.; Fernandes, A.; Lopes, A.; Pinheiro, H.; Goncalves, I. Electrochemical degradation applied to the metabolites of Acid Orange 7 anaerobic biotreatment. *Chemosphere* **2007**, *67*, 1316–1324. [CrossRef]

51. Konstantinou, I.K.; Albanis, T.A. TiO_2-assisted photocatalytic degradation of azo dyes in aqueous solution: Kinetic and mechanistic investigations. *Appl. Catal. B Environ.* **2009**, *49*, 1–14. [CrossRef]

52. Hamidian, K.; Najafidoust, A.; Miri, A.; Sarani, M. Photocatalytic performance on degradation of Acid Orange 7 dye using biosynthesized un-doped and Co doped CeO_2 nanoparticles. *Mater. Res. Bull.* **2021**, *138*, 111206. [CrossRef]

53. Hamidian, K.; Rigi, A.H.; Najafidoust, A.; Sarani, M.; Miri, A. Study of photocatalytic activity of green synthesized nickel oxide nanoparticles in the degradation of acid orange 7 dye under visible light. *Bioprocess Biosyst. Eng.* **2021**, *44*, 2667–2678. [CrossRef]

54. Xian, T.; Sun, X.; Di, L.; Li, H.; Yang, H. Improved photocatalytic degradation and reduction performance of Bi_2O_3 by the decoration of AuPt alloy nanoparticles. *Opt. Mater.* **2021**, *111*, 110614. [CrossRef]

55. Mancuso, A.; Sacco, O.; Vaiano, V.; Bonelli, B.; Esposito, S.; Freyria, F.S.; Blangetti, N.; Sannino, D. Visible light-driven photocatalytic activity and kinetics of Fe-doped TiO_2 prepared by a three-block copolymer templating approach. *Materials* **2021**, *14*, 3105. [CrossRef] [PubMed]

56. Rodrigues, A.; Jorge, M.E.M.; Ciríaco, L.; Pacheco, M.J.; Lopes, A. Perovskites (La,Ba)(Fe,Ti)O_3: AO7 photocatalysis under visible light. *Rev. Adv. Mater. Sci.* **2020**, *59*, 151–159. [CrossRef]